CHEMISTRY OF MATERIALS

Article

pubs.acs.org/cm

Synthesis of a 4,9-Didodecyl Angular-Shaped Naphthodiselenophene Building Block To Achieve High-Mobility Transistors

Che-En Tsai, Ruo-Han Yu, Fang-Ju Lin, Yu-Ying Lai, Jhih-Yang Hsu, Sheng-Wen Cheng, Chain-Shu Hsu,* and Yen-Ju Cheng*

Department of Applied Chemistry, National Chiao Tung University, 1001 University Road, Hsin-Chu 30010, Taiwan

Supporting Information

ABSTRACT: A new tetracyclic 4,9-dialkyl angular-shaped naphthodiselenophene (4,9-α-aNDS) was designed and synthesized. The naphthalene core in 4,9-α-aNDS is formed by the DBU-induced 6π-cyclization of an (*E*)-1,2-bis(3-(tetradec-1-yn-1-yl)selenophen-2-yl)ethene intermediate followed by the second $PtCl_2$-catalyzed benzannulation. This synthetic protocol allows for incorporating two dodecyl groups regiospecifically at 4,9-positions of the resulting α-aNDS. An ordered supramolecular self-assembly formed via noncovalent selenium−selenium interactions with a short contact of 3.5 Å was observed in the single-crystal structure of 4,9-α-aNDS. The distannylated α-aNDS building block was copolymerized with Br-DTFBT and Br-DPP acceptors by Stille cross coupling to form two new donor−acceptor polymers PαNDSDTFBT and PαNDSDPP, respectively. The bottom-gate/top-contact organic field-effect devices using the PαNDSDTFBT and PαNDSDPP semiconductors accomplished superior hole mobility of 3.77 and 2.17 $cm^2\ V^{-1}\ s^{-1}$, respectively, which are among the highest mobilities reported to date.

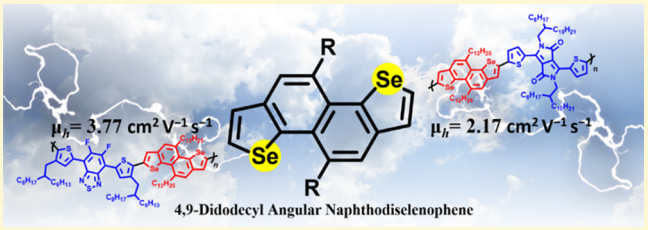

INTRODUCTION

Ladder-type conjugated structures with rigid and coplanar molecular frameworks feature longer effective conjugation, narrow optical bandgap, and strong intermolecular $\pi-\pi$ interactions which are ideal characteristics for organic field-effect transistors (OFETs).[1−19] Acenedithiophenes, made up of linearly fused benzene rings with two terminal thiophenes, are particularly superior building blocks due to their coplanar structures, facile functionalization, and high charge mobility. Benzodithiophene (BDT)-incorporating donor−acceptor (D-A) copolymers have achieved high-efficiency solar cells,[20−25] whereas anthradithiophene (ADT) derivatives have shown high mobilities in *p*-type OFETs[26−32] More recently, growing research effort is directed toward the synthesis and molecular properties of naphthodithiophenes (NDT) having versatile isomeric structures.[33−37] In addition to the linear-shaped NDTs, angular-shaped NDTs (aNDT) can have two α-aNDT and β-aNDT isomers (see Chart 1). Takimiya and Osaka et al. first incorporated alkyl chains into an α-aNDT to ensure the solubility of the resulting polymers for solution-processable transistors and solar cells.[38,39] We recently described a synthetic strategy to introduce two alkyl groups at 4,9- or 5,10-positions of both α-aNDT and β-aNDT.[40] It has been demonstrated that the isomeric geometry of the NDT moiety governs the polymeric packing and ordering, which ultimately affects the macroscopic device performance.[41,42] Compared to the dialkyl β-aNDT-based analogues, the D-A copolymers incorporating dialkyl α-aNDT units exhibited more linear polymer backbones, thereby leading to the superior photovoltaic efficiency and transistor mobility.[41,42]

Chart 1. Chemical Structures of α-aNDT, β-aNDT, α-aNDS, β-aNDS, 4,9-Didodecyl α-aNDT and 4,9-Didodecyl α-aNDS in This Research

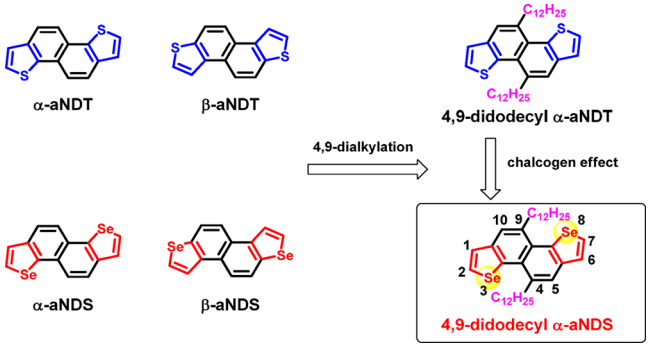

Selenophene generally has similar chemical and physical properties with thiophene in the chalcogenophene family. However, selenophene possesses several distinct and promising features that are desirable for developing a new generation of organic semiconductors.[43−55] Theoretical and experimental results suggest that polyselenophene adopts more quinoidal

Received: May 20, 2016
Revised: June 30, 2016

DOI: 10.1021/acs.chemmater.6b02042
Chem. Mater. XXXX, XXX, XXX−XXX

Scheme 1. Synthetic Route toward Sn-4,9-α-aNDS

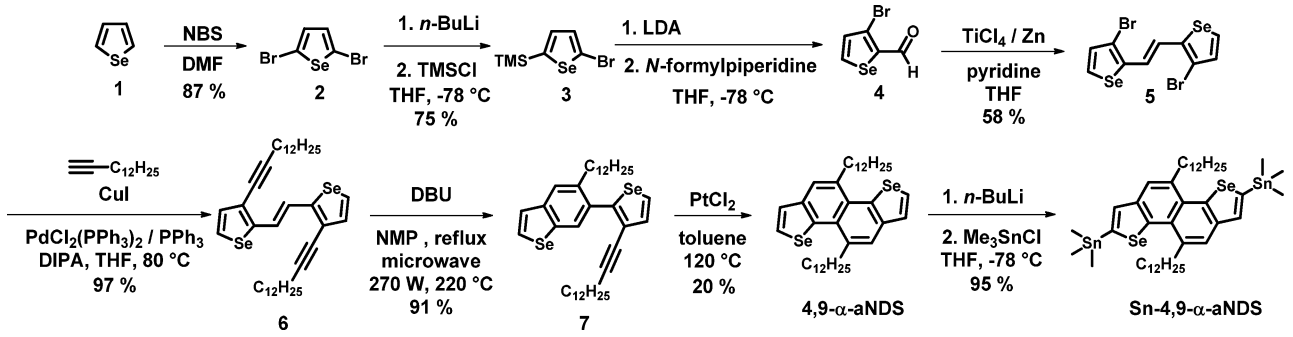

Scheme 2. Synthesis of PαNDSDTFBT and PαNDSDPP Donor−Acceptor Copolymers

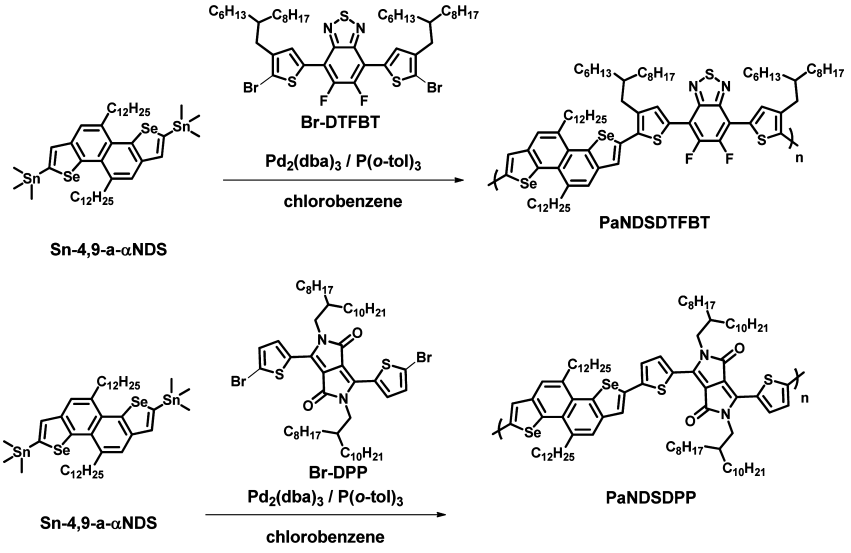

character and thus less backbone twisting than polythiophene, resulting in longer effective conjugation length and stronger intermolecular interactions.[56−58] Higher polarizability of selenium might induce intermolecular selenium−selenium (Se−Se) interaction[59,60] or selenium−aromatic interaction[61] in the selenophene-containing molecules. Consequently, the selenophene-based materials have been demonstrated to show enhanced light-harvesting ability and improved charge carrier mobility in comparison with the corresponding thiophene-based counterparts. These beneficial features prompt us to further develop a dialkylated angular-shaped naphthodiselenophene (aNDS) by replacing thiophene in aNDT with selenophene. Despite the synthesis of the bare aNDS derivatives has been sporadically described, its utilization in polymer semiconductors has never been explored due to the poor solubility as well as the fact that functionalization of selenophene derivatives is synthetically more challenging.[62,63] To impart solubility for diverse applicability, it is of importance to implant alkyl solubilizing groups into the aNDS framework. In this research, we present a useful methodology to synthesize successfully the 4,9-didodecyl α-aNDS monomer (simplified as 4,9-α-aNDS in Scheme 1) where the placement of the side chain on the central naphthalene moiety and the geometry of the fused thiophenes can be regiospecifically controlled. Its distannylated monomer was copolymerized with the Br-DTFBT and Br-DPP acceptors to form two new alternating donor−acceptor copolymers, PαNDSDTFBT and PαNDSDPP, respectively. Their molecular properties and transistor characteristics will be presented and discussed.

RESULTS AND DISCUSSION

Synthesis. The synthetic route for α-aNDS is shown in Scheme 1. Bromination of selenophene (1) yielded 2,5-dibromoselenophene (2). Lithiation of 2 by *n*-BuLi to react with trimethylsilyl chloride (TMSCl) resulted in compound 3. Treatment of 3 with lithium diisopropylamide (LDA) followed by quenching with *N*-formylpiperidine furnished compound 4. McMurry coupling of 4 in the presence of $TiCl_4$/ZnO afforded the dimerized compound 5 with *E*-form olefin configuration as the major product in 58% yield. Sonogashira coupling reaction of compound 5 with tetradec-1-yne yielded compound 6 in almost quantitative yield. In the presence of 1,8-diazabicyclo[5.4.0]undec-7-ene (DBU) with microwave irradiation, compound 6 underwent an intramolecular benzannulation to form compound 7. The mechanism involves propargyl-allenyl isomerization followed by 6π-electrocyclization/aromatization.[37,64] $PtCl_2$-catalyzed benzannulation of 7 via a 6-endo-dig fashion afforded 4,9-α-aNDS with two dodecyl groups regiospecifically at the 4,9-postions. 4,9-α-aNDS was further stannylated to yield the target Sn-4,9-α-aNDS monomer in a high yield of 95%. Sn-4,9-α-aNDS was polymerized with Br-DTFBT and Br-DPP monomers to form two alternating donor−acceptor copolymers, PαNDSDTFBT and PαNDSDPP, respectively (Scheme 2).

DOI: 10.1021/acs.chemmater.6b02042
Chem. Mater. XXXX, XXX, XXX−XXX

Single-Crystal Structure Analysis of 4,9-α-aNDS. The chemical structure of 4,9-α-aNDS is unambiguously confirmed by its single-crystal X-ray crystallography and is shown in Figure 1. An ordered supramolecular self-assembly is established along the *b* axis through noncovalent selenium−selenium (Se−Se) interactions with a short contact of 3.5 Å, which is smaller than the sum of van der Waals radius for two Se (2 Å for one Se). To the best of our knowledge, this is the first time that the Se−Se noncovalent interactions can be observed in a selenophene-containing molecule. It should be noted that the corresponding 4,9-α-aNDT molecule does not have similar sulfur−sulfur interactions in its single-crystal structure,[40] suggesting that the high polarizability of selenium might be an important characteristic to induce such interactions.

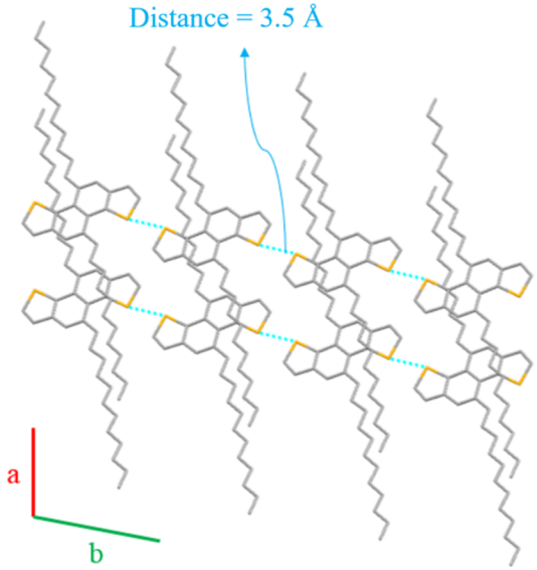

Figure 1. Single-crystal structure and molecular packing of 4,9-α-aNDS by X-ray crystallography.

Theoretical Calculations Based on the Single-Crystal Structure. The crystal packing of 4,9-α-aNDS reveals that the direction of π stacking is in line with the *a* unit-cell axis and Se−Se short contacts are in plane with the *b* axis (Figure 2a). Extended transition state-natural orbitals for chemical valence (ETS-NOCV) analysis[65−67] was then performed to gain insight into the dimeric intermolecular interactions along the *a* and *b* axes in the 4,9-α-aNDS single-crystal structure, named as t_a and t_b (Figure 2b), respectively. The ETS-NOCV results calculated at the BP86-BJDAMP/TZP level of theory are summarized in Table 1. The magnitude of interaction energy (ΔE_{int}) is utilized to quantify the strength of intermolecular interactions. Under this theoretical framework, ΔE_{int} is the sum of Pauli repulsion (ΔE_{Pauli}), electrostatic interaction (ΔV_{elst}), orbital interaction (ΔE_{oi}), and dispersion (ΔE_{dis}). Through computational decomposition of ΔE_{int}, the estimation of each contribution was obtained. More information about ETS-NOCV is described in the Supporting Information. As listed in Table 1, ΔE_{int} (t_a) (−38.60 kcal mol^{-1}) is much larger than ΔE_{int} (t_b) (−6.76 kcal mol^{-1}), suggesting that the intermolecular interactions along the π stacking is greater than those along the *b* axis containing Se−Se short contacts. For both t_a and t_b, the major contribution comes from the dispersion term rather than the electrostatic or orbital interaction, which is consistent with the direct interaction model, proposed by Sherrill and co-workers, accounting for the π stacking of aromatics.[68−70] The computational results in Table 1 reveal that the ΔE_{dis} (64%) contributes most significantly in t_b. The observation of the unique Se−Se short contacts in the 4,9-α-aNDS single-crystal structure is highly associated with the high polarizability of selenium to induce stronger dispersion force.

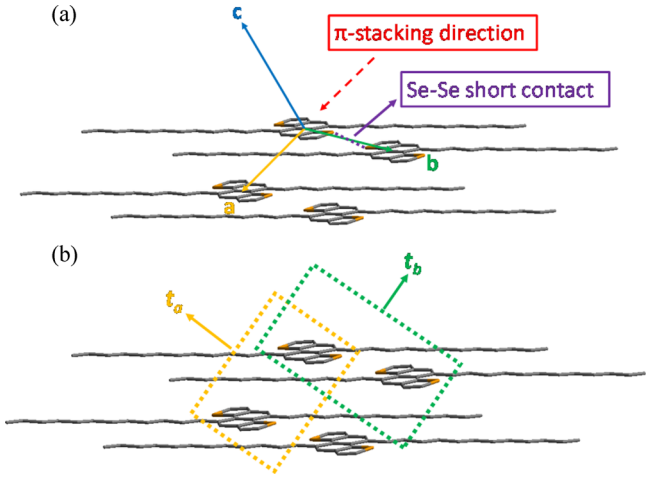

Figure 2. (a) Illustration for crystal packing of 4,9-α-aNDS; (b) t_a, two 4,9-α-aNDS molecules in the orange rectangle; t_b, two 4,9-α-aNDS molecules in the green rectangle. Deep orange, selenium; gray, carbon; hydrogen are omitted for clarity.

Visualization of the Se−Se orbital interactions can be realized by the deformation-density operation in ETS-NOCV. Figure 3 displays two deformation-density contributions that describe the Se−Se bonding. The green area stands for the electron-density accumulation, whereas the red area denotes the electron-density depletion. Figure 3a depicts the electron donation from the Se−C bond in one 4,9-α-aNDS molecule into the Se atom in the adjacent 4,9-α-aNDS molecule. Conversely, Figure 3b represents the electron donation from Se in one 4,9-α-aNDS into the Se−C bond in the other molecule. The overall stabilization energy for the Se−Se orbital interactions is estimated to be −1.52 kcal mol^{-1} (−0.82 kcal mol^{-1} + −0.70 kcal mol^{-1}).

UV−vis Absorption. The absorption spectra of 4,9-α-aNDS and 4,9-α-aNDT small molecules are shown in Figure 4. Despite the similar absorption profiles, 4,9-α-aNDS exhibited a more bathochromic absorption maxima at 279 nm than 4,9-α-aNDT at 288 nm, which may result from the better electron delocalization ability of selenophene. The optical band gaps (E_g^{opt}) calculated from the absorption edges are determined to be 3.35 eV for 4,9-α-aNDT and 3.28 eV for 4,9-α-aNDS. The absorption spectra of polymers PαNDSDTFBT and PαNDSDPP in solutions and thin films are shown in Figure 5. PαNDSDTFBT showed an absorption maximum at 617 nm, whereas PαNDSDPP using stronger electron-withdrawing DPP acceptor exhibited the apparent bathochromic shift of the intramolecular charge transfer (ICT) band at 751 nm in the solution. PαNDSDTFBT exhibited *ca.* 50 nm red-shifted λ_{max} from solution to solid state, whereas PαNDSDPP is essentially unchanged. This result implies that PαNDSDTFBT might has stronger interactions in the solid state. The optical band gaps (E_g^{opt}) calculated from the absorption edges of the solid state spectra are determined to be 1.60 eV for PαNDSDTFBT and 1.39 eV for PαNDSDPP.

DOI: 10.1021/acs.chemmater.6b02042
Chem. Mater. XXXX, XXX, XXX−XXX

Table 1. BP86-BJDAMP/TZP ETS-NOCV Analysis of the Dimeric Intermolecular Interactions in kcal mol^{-1} along the *a* and *b* Unit-Cell Axes in the 4,9-*α*-aNDS Crystal Structure[a]

direction	ΔE_{int}	ΔE_{Pauli}	ΔV_{elst}	ΔE_{oi}	ΔE_{dis}
t_a	−38.60	22.11	−8.78 (14%)	−6.48 (11%)	−45.45 (75%)
t_b	−6.76	7.18	−2.34 (17%)	−2.65 (19%)	−8.95 (64%)

[a]Percentage of total stabilization is given in parentheses.

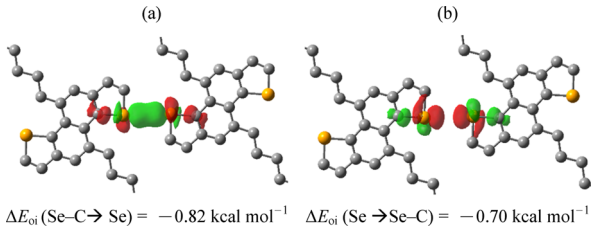

Figure 3. Contours of deformation density (isosurface density = 0.0004 au) contributions describing the Se−Se orbital interactions observed in the crystal packing of 4,9-*α*-aNDS. (a) Electron donation from the Se−C bond in 4,9-*α*-aNDS into the Se in the other molecule. (b) Electron donation from Se in one 4,9-*α*-aNDS into the Se−C bond in the other molecule. Green area stands for the electron-density accumulation; red area denotes the electron-density depletion. For clarity, hydrogens and part of aliphatic side chains are omitted.

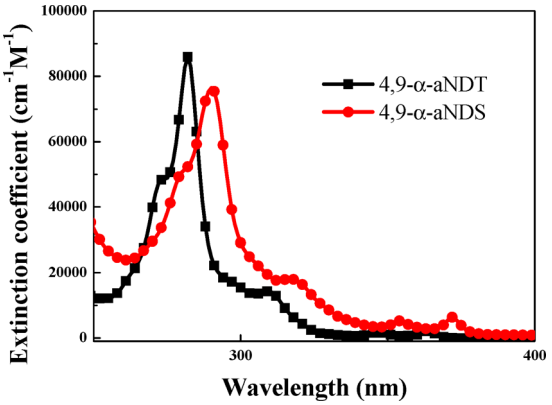

Figure 4. Absorption spectra of 4,9-*α*-aNDS and 4,9-*α*-aNDT in chloroform with concentration of ca. 5 × 10^{-6} M.

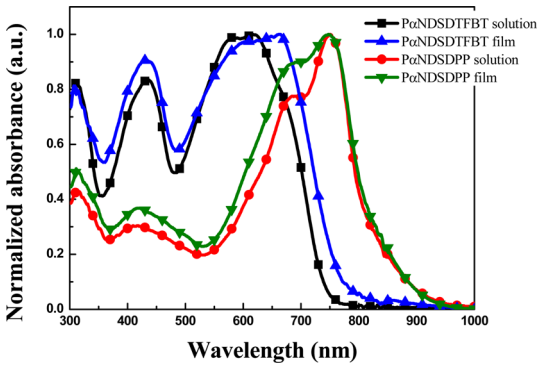

Figure 5. Normalized absorption spectra of P*α*NDSDTFBT and P*α*NDSDPP in *ortho*-dichlorobenzene solutions and thin films.

Thermal Properties. The thermal stability of two polymers was measured by thermogravimetric analysis (TGA). P*α*NDSDTFBT and P*α*NDSDPP showed sufficiently high decomposition temperatures (T_d) of 408, and 414 °C, respectively (Figure 6).

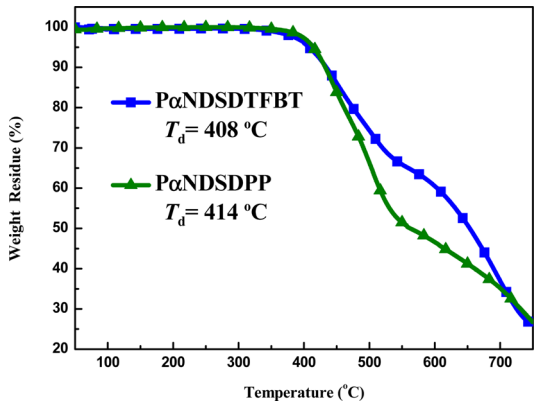

Figure 6. Thermogravimetric analysis of P*α*NDSDTFBT and P*α*NDSDPP at a ramping rate of 10 °C/min.

Electrochemical Properties. Cyclic voltammetry (CV) was used to examine the electrochemical properties and evaluate the HOMO/LUMO levels and the electronic band gaps of 4,9-*α*-aNDS and 4,9-*α*-aNDT and the polymers (Table 2 and Figure 7). The two polymers showed reversible and stable processes in the oxidative scans, which are important prerequisites for organic OFET and PSC applications. The HOMO energy levels are estimated to be −5.78 and −5.74 eV for 4,9-*α*-aNDS and 4,9-*α*-aNDT; and −5.41 and −5.43 eV for P*α*NDSDTFBT and P*α*NDSDPP, respectively. It is worth noting that compared to other DPP-based polymers, the HOMO level of P*α*NDSDPP is relatively low which is attributed to the lower-lying HOMO level of the 4,9-*α*-aNDS (−5.78 eV). On the other hand, the LUMO energy levels are approximately located at −3.56 eV for P*α*NDSDTFBT and −3.84 eV for P*α*NDSDPP.

Transistor Characteristics. The OFET mobilities of the two *α*-aNDS-based polymers were measured by fabricating the OFET bottom-gate/top-contact devices with evaporated gold source/drain electrodes (40 nm in thickness). The devices were modified with a self-assembled octadecyltrichlorosilane (ODTS) monolayer on the SiO_2 as the gate dielectric. The output and transfer plots of the devices showed typical p-type OFET characteristics (Figure 8 and Table 3).

The hole mobilities are calculated from the transfer characteristics of the devices in the saturation regime. After thermal annealing at 200 °C for 10 min, P*α*NDSDPP exhibited a prominent mobility of 2.17 cm^2 V^{-1} s^{-1}. More encouragingly, P*α*NDSDTFBT delivered an even higher hole mobility of up to 3.77 cm^2 V^{-1} s^{-1}.

Grazing Incidence X-ray Scattering (GIXS). The polymeric orientation and packing in the thin-films annealed at 200 °C for 10 min were investigated by grazing-incidence X-ray scattering (GIXS). In-plane 1D diffraction patterns of the polymer thin films are shown in Figure 9a. P*α*NDSDPP showed (100) and (200) peaks that are assignable to a lamellar *d*-spacing (d_1) of ca. 24 Å corresponding to the interdigitation of side chains between two polymeric backbones. Meanwhile,

DOI: 10.1021/acs.chemmater.6b02042
Chem. Mater. XXXX, XXX, XXX−XXX

Table 2. Summary of the Intrinsic Properties of the Polymers

materials	M_n (kDa)	PDI (M_w/M_n)	λ_{max} (nm) oDCB[c]	λ_{max} (nm) film	HOMO (eV)	LUMO (eV)	$^aE_g^{ele}$ (eV)	$^bE_g^{opt}$ (eV)	T_d (°C)
4,9-α-aNDS			288		−5.78	−2.50		3.28	
4,9-α-aNDT			279		−5.74	−2.39		3.35	
PαNDSDTFBT	33.3	1.29	437, 582, 617	432, 604, 665	−5.41	−3.56	1.85	1.60	408
PαNDSDPP	107.1	3.94	419, 691, 751	422, 686, 748	−5.43	−3.84	1.59	1.39	414

[a]E_g^{ele} was determined from cyclic voltammetry by subtracting the HOMO energy value from the LUMO energy value. [b]E_g^{opt} was estimated from the onset of UV−vis absorption in the solid state. *o*DCB is *ortho*-dichlorobenzene.

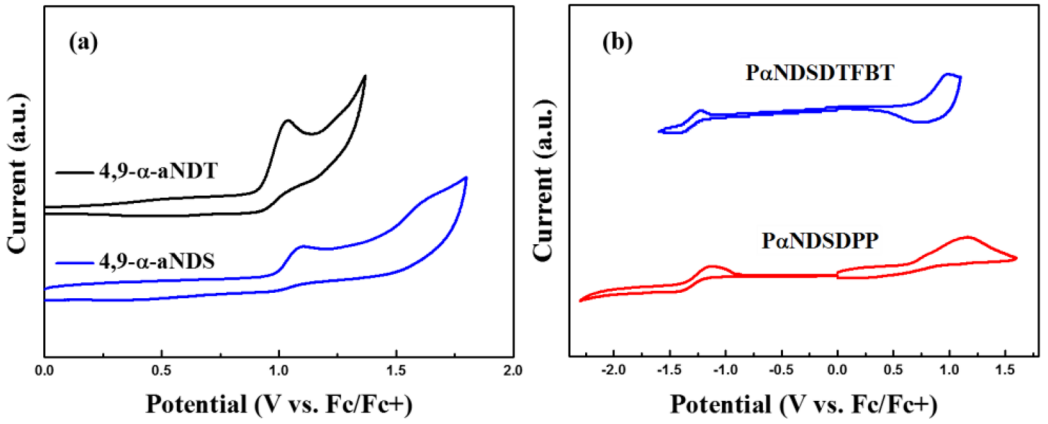

Figure 7. Cyclic voltammograms of (a) 4,9-α-aNDS and 4,9-α-aNDT in the chloroform; (b) PαNDSDTFBT and PαNDSDPP in the thin films at a scan rate of 100 mV/s.

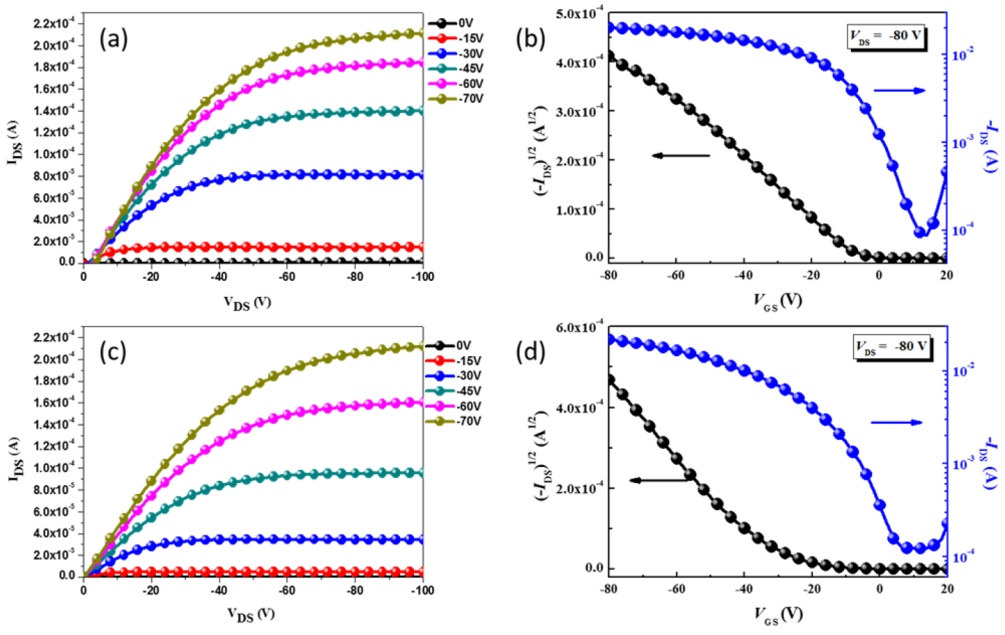

Figure 8. Typical output curves (a, c) and transfer plots (b, d) of the OFET devices based on PαNDSDTFBT and PαNDSDPP, respectively.

Table 3. OFET Characteristics of the Polymer Thin Films

copolymer	$I_{on/off}$	V_{th} (V)	mobility ($cm^2\ V^{-1}\ s^{-1}$)
PαNDSDTFBT	10^4−10^5	−1.38	3.77 (2.77 ± 0.35)[a]
PαNDSDPP	10^4−10^5	−9.60	2.17 (2.06 ± 0.05)[a]

[a]Average value of 10 devices with standard deviation.

PαNDSDPP also showed a weak peak at q_z = 1.69 $Å^{-1}$ corresponding to π-stacking between two facing conjugated backbones with a distance (d_π) of ca. 3.7 Å. On the other hand, PαNDSDTFBT exhibited much stronger in-plane (100) and (200) peaks that correspond to a shorter lamellar *d*-spacing (d_l) of ca. 17 Å than that of PαNDSDPP. To gain more insight on the polymer conformation and intermolecular packing, theoretical calculations were conducted on two model compounds composed of two D-A repeating units, denoted as 2NDSDPP and 2NDSDTFBT. The optimized geometries of 2NDSDPP and 2NDSDTFBT were thus utilized to fit the ordered lamellar packing through the side-chain interdigitation (Figure 9b,c). It is found that the two branched 2-hexyldecyl

DOI: 10.1021/acs.chemmater.6b02042
Chem. Mater. XXXX, XXX, XXX−XXX

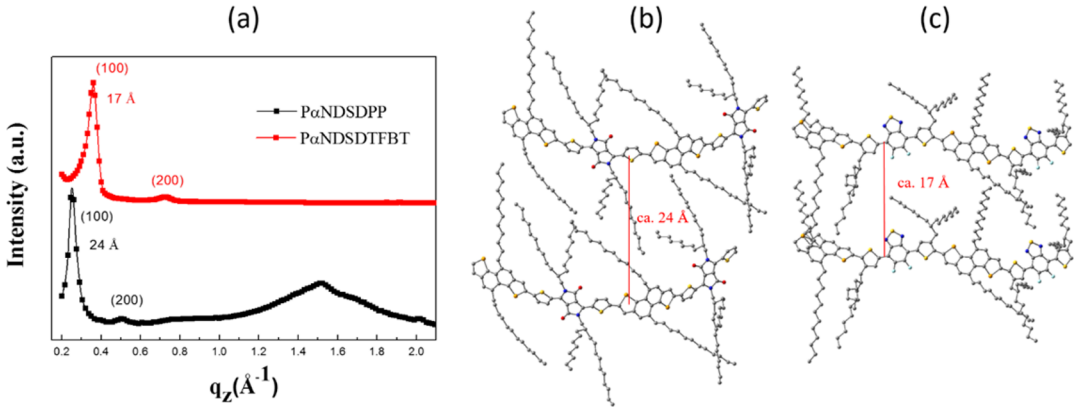

Figure 9. (a) GIXS in-plane patterns of PαNDSDPP and PαNDSDTFBT thin films. The schematic dimeric structures of (b) 2NDSDPP and (c) 2NDSDTFBT to simulate the lamellar packing of PαNDSDPP and PαNDSDTFBT.

groups at the thienyl units connected to the central FBT unit stretch out at the opposite directions in order to avoid the steric hindrance. Such backbone conformations and side-chain arrangements enable PαNDSDTFBT to have closer lamellar packing in comparison with PαNDSDPP. The thin film GIXS patterns revealed that both polymers have ordered packing structures, leading to the high mobility of 3.77 $cm^2\ V^{-1}\ s^{-1}$ for PαNDSDTFBT and 2.17 $cm^2\ V^{-1}\ s^{-1}$ for PαNDSDPP.

CONCLUSIONS

We have successfully synthesized a new angular-shaped and α-form naphthodiselenophene conjugated architecture (4,9-α-aNDS) with two dodecyl groups substituted at 4,9-positions. The naphthalene core in 4,9-α-aNDS is constructed by a DBU-induced 6π-cyclization of an (*E*)-1,2-bis(3-(tetradec-1-yn-1-yl)selenophen-2-yl)ethene intermediate followed by a $PtCl_2$-catalyzed benzannulation. 4,9-α-aNDS shows a more red-shifted absorption spectrum and stronger intermolecular interactions than the corresponding 4,9-α-aNDT analogous. Single-crystal structure reveals that 4,9-α-aNDS is self-assembled by the noncovalent Se−Se interactions with a short contact of 3.5 Å due to the high polarizability of selenium. To the best of our knowledge, this is the first time that the Se−Se interactions have ever been observed in a selenophene-containing molecule. The distannylated α-aNDS was copolymerized by Stille cross-coupling with the Br-DTFBT and Br-DPP acceptor to form two new donor−acceptor copolymers PαNDSDTFBT and PαNDSDPP, respectively. The bottom-gate/top-contact OFET devices using PαNDSDTFBT and PαNDSDPP semiconductors achieved the eminent mobility of 3.77 and 2.17 $cm^2\ V^{-1}\ s^{-1}$, respectively. This work demonstrates that the new 4,9-dialkyl α-aNDS is a superior building block for making a variety of promising solution-processable semiconductor materials.

EXPERIMENTAL SECTION

General Measurements and Characterization. ^1H and ^{13}C NMR spectra were measured using a Varian 400 MHz instrument spectrometer and obtained in deuterated chloroform ($CDCl_3$) with TMS as internal reference unless otherwise stated, and chemical shifts (δ) are reported in parts per million. Absorption spectra were taken on a HP8453 UV−vis spectrophotometer. Thermal gravimetric analyzer (TGA) was measure on a PerkinElmer Pyris Instrument with heating rate of 10 °C/min from 50 to 750 °C after preheating at 110 °C for 10 min. Electrochemical cyclic voltammetry was conducted on a CH instruments electrochemical analyzer. A carbon glass was used as the working electrode, Pt wire was used as the counter electrode, and Ag/Ag^+ electrode (0.01 M $AgNO_3$, 0.1 M TBAP in acetonitrile) was used as the reference electrode in a solution of dichloromethane with 0.1 M $TBAPF_6$ (tetrabutylammonium hexafluorophosphate) at 100 mV/s. CV curves were calibrated using ferrocene as the standard, whose HOMO is set at −4.8 eV with respect to zero vacuum level. The HOMO energy levels were obtained from the equation HOMO = $-(E_{ox}^{onset} - E_{(ferrocene)}^{onset} + 4.8)$ eV. The LUMO levels were obtained from the equation LUMO = $-(E_{red}^{onset} - E_{(ferrocene)}^{onset} + 4.8)$ eV. The molecular weights of the polymers were determined by a Viscotek VE2001 GPC, and polystyrene was used as the standard and THF as the eluent. GIXS experiments were conducted at National Synchrotron Radiation Research Center on beamline BL23A in Taiwan. The samples were irradiated with an X-ray energy of 10.09 keV (λ = 1.23 Å) at a fixed incident angle of 0.08° through a coupled double crystal Si(111)/multilayer (Mo/B_4C) monochromator, and the GIXS patterns were recorded on a 2D image detector (Pilatus 1M-F area detector). The polymer films for GIXS measurement were prepared under the same condition used for the OFET device. 4,9-Didodecyl α-aNDT,[42] 2,5-dibromoselenophene (2) and 2-bromo-5-trimethylsilylselenophene (3)[71] were synthesized as reported.

*Synthesis of 3-Bromoselenophene-2-carbaldehyde (**4**).* To an anhydrous THF (110 mL) solution of 3 (5.00 g, 17.72 mmol) was added lithium diisopropylamide (LDA) (9.75 mL, 2 M) slowly at −78 °C. After stirring for 1.5 h at −78 °C, *N*-formylpiperidine (2.36 mL, 21.27 mmol) was added and stirred for 30 min at −78 °C. The mixture was warmed to rt and stirred for 2 h, and then was quenched by the saturated NH_4Cl solution. The organic layer was separated and the aqueous layer was extracted with EA (20 mL × 3). The combined organic layer was dried over anhydrous $MgSO_4$. After filtration, the solvent was removed under vacuum. The residue was purified by column chromatography on silica gel (hexane/EA = 20/1) to give a brown solid 4 (3.23 g, yield: 77%). ^1H NMR ($CDCl_3$, 400 MHz): δ 9.87 (s, 1 H), 8.40 (d, J = 6.4 Hz, 1 H), 7.42 (d, J = 6.4 Hz, 1 H). ^{13}C NMR ($CDCl_3$, 100 MHz): δ 184.4, 142.0, 140.3, 134.9, 120.9. HRMS (ESI, C_5H_3BrOSe + H): calcd, 238.8611; found, 238.8602.

*Synthesis of (E)-1,2-Bis(3-bromoselenophen-2-yl)ethane (**5**).* To a three-necked round-bottomed flask with anhydrous THF (88 mL), $TiCl_4$ (3.48 mL, 31.52 mmol) was slowly added and the mixture was stirred at 0 °C for 15 min. Zinc powder (4.12 g, 63.04 mmol) was then added portion-wise, and the reaction mixture was refluxed for 1h. After cooling to 0 °C, compound **4** (5.00 g, 21.01 mmol) and pyridine (2.54 mL, 31.52 mmol) were added. The mixture was refluxed for 12 h, and then quenched by water (50 mL) and hydrochloric acid (1 M, 10 mL). The mixture was extracted with EA (20 mL × 3). The combined organic layer was dried over anhydrous $MgSO_4$. After filtration, the solvent was removed under vacuum. The residue was purified by column chromatography on silica gel (hexane/EA = 10/1) to give a yellow solid **5** (2.70 g, yield: 58%). ^1H NMR ($CDCl_3$, 400 MHz): δ 7.81 (d, J = 6.0 Hz, 2 H), 7.21 (d, J = 6.0 Hz, 2 H), 7.07 (s, 2 H). ^{13}C

DOI: 10.1021/acs.chemmater.6b02042
Chem. Mater. XXXX, XXX, XXX−XXX

NMR ($CDCl_3$, 100 MHz): δ 140.8, 133.8, 128.6, 125.0, 112.5. HRMS (APPI, $C_{10}H_6Br_2Se_2$): calcd, 443.7165; found, 443.7154.

*Synthesis of (E)-1,2-Bis(3-(tetradec-1-yn-1-yl)selenophen-2-yl)-ethane (**6**).* To a deoxygenated solution of compound **5** (2.60 g, 5.86 mmol) in THF (50 mL) and diisopropylamine (50 mL) was added $Pd(PPh_3)_2Cl_2$ (1.03 g, 1.46 mmol, 25 mol %), CuI (280 mg, 1.46 mmol, 25 mol %), PPh_3 (380 mg, 1.46 mmol, 25 mol %) and tetradec-1-yne (3.42 g, 17.57 mmol). The mixture was stirred at 80 °C for 12 h, and filtered by Celite. The resulting mixture was added to the saturated NH_4Cl solution, and extracted with EA (10 mL × 3). The combined organic layer was dried over anhydrous $MgSO_4$, filtered, and concentrated in vacuum. The residue was purified by column chromatography on silica gel (hexane) to give a yellow solid **6** (3.81 g, yield: 97%). ^{1}H NMR ($CDCl_3$, 400 MHz): δ 7.68 (d, J = 5.6 Hz, 2 H), 7.27 (s, 2 H), 7.18 (d, J = 5.6 Hz, 2 H), 2.46 (t, J = 7.0 Hz, 4 H), 1.66−1.63 (m, 4 H), 1.52−1.48 (m, 4 H), 1.37−1.26 (m, 36 H), 0.88 (t, J = 6.8 Hz, 6 H). ^{13}C NMR ($CDCl_3$, 100 MHz): δ 149.8, 133.1, 126.9, 124.8, 124.2, 95.1, 76.4, 31.9, 29.68, 29.67, 29.64, 29.56, 29.3, 29.2, 29.0, 28.8, 22.7, 19.7, 14.1. HRMS (APPI, $C_{38}H_{56}Se_2$ + H): calcd, 673.2788; found, 673.2793.

*Synthesis of 5-Dodecyl-6-(3-(tetradec-1-yn-1-yl)selenophen-2-yl)-benzo[b]selenophene (**7**).* To a deoxygenated *N*-methyl-2-pyrrolidone (NMP, 10 mL) solution of compound **6** (1.00 g, 1.49 mmol) was added 1,8-diazabicycloundec-7-ene (DBU) (0.45 mL, 2.98 mmol). The reaction was refluxed in the focused microwave instrument under 270 W for 1 h, and then cooled to rt. The resulting mixture was diluted with water (20 mL), and extracted with EA (10 mL × 3). The combined organic layer was washed with brine solution (5 mL) and dried over anhydrous $MgSO_4$. After filtration, the solvent was removed under vacuum and the residue was purified by column chromatography on silica gel (hexane) to give a yellow solid **7** (0.91 g, yield: 91%). ^{1}H NMR ($CDCl_3$, 400 MHz): δ 7.97 (d, J = 6.0 Hz, 1 H), 7.90 (d, J = 6.0 Hz, 1 H), 7.88 (s, 1 H), 7.71 (s, 1 H), 7.53 (d, J = 6.0 Hz, 1 H), 7.32 (d, J = 6.0 Hz, 1 H), 2.77 (t, J = 8.0 Hz, 4 H), 2.17 (t, J = 7.0 Hz, 4 H), 1.37−1.10 (m, 40 H), 0.91−0.87 (m, 6 H). ^{13}C NMR ($CDCl_3$, 100 MHz): δ 150.8, 142.3, 138.8, 137.7, 132.5, 131.9, 129.3, 128.8, 127.9, 127.4, 125.3, 123.9, 91.4, 33.5, 31.95, 31.94, 30.96, 29.7, 29.6, 29.5, 29.46, 29.43, 29.40, 29.38, 29.1, 28.6, 22.71, 22.70, 19.3, 14.1. HRMS (APPI, $C_{38}H_{56}Se_2$ + H): calcd, 673.2796; found, 673.2793.

Synthesis of 4,9-Didodecylnaphtho[1,2-b:5,6-b′]bis(selenophene) (4,9-α-aNDS). To a deoxygenated toluene (10 mL) solution of compound **7** (200 mg, 0.30 mmol) was added $PtCl_2$ (3.97 mg, 0.015 mmol), and stirred at 120 °C for 36 h. The resulting mixture was filtered by Celite, and concentrated under vacuum. The residue was purified by column chromatography on silica gel (hexane), and recrystallized from CH_2Cl_2/MeOH to give a slight yellow needle 4,9-α-aNDS (42 mg, yield: 20%). ^{1}H NMR ($CDCl_3$, 400 MHz): δ 8.17 (d, J = 6.0 Hz, 2 H), 7.94 (s, 2 H), 7.77 (d, J = 6.0 Hz, 2 H), 3.41 (t, J = 8.0 Hz, 4 H), 1.92−1.86 (m, 4 H), 1.64−1.59 (m, 4 H), 1.44−1.27 (m, 36 H), 0.88 (t, J = 6.8 Hz, 6 H). ^{13}C NMR ($CDCl_3$, 100 MHz): δ 139.8, 135.9, 135.8, 130.4, 129.4, 128.1, 125.0, 36.6, 31.9, 31.1, 29.9, 29.7, 29.6, 29.4, 22.7, 14.1. HRMS (APPI, $C_{38}H_{56}Se_2$ + H): calcd, 673.2798; found, 673.2793.

Synthesis of (4,9-Didodecylnaphtho[1,2-b:5,6-b′]bis-(selenophene)-2,7-diyl)bis(trimethylstannane) (Sn-4,9-α-aNDS). To an anhydrous THF (7.5 mL) solution of 4,9-α-aNDS (120 mg, 0.18 mmol) was added *n*-butyllithium (0.22 mL, 2.5 M) slowly at −78 °C. After stirring for 30 min at −78 °C, trimethyltin chloride (0.72 mL, 1 M) was added. The mixture was warmed to rt and stirred for 12 h, and then quenched with the saturated NH_4Cl solution (10 mL). The organic layer was separated and the aqueous layer was extracted with EA (5 mL × 3). The combined organic extract was washed with brine solution (10 mL) and dried over anhydrous $MgSO_4$. After filtration, the solvent was removed under vacuum, and the residue was recrystallized from CH_2Cl_2/MeOH to give a slight yellow needle Sn-4,9-α-aNDS (170 mg, yield: 95%). ^{1}H NMR ($CDCl_3$, 400 MHz): δ 7.93 (s, 2 H), 7.92 (s, 2 H), 3.43 (t, J = 7.8 Hz, 4 H), 1.93−1.85 (m, 4 H), 1.66−1.58 (m, 4 H), 1.43−1.27 (m, 36 H), 0.88 (t, J = 6.8 Hz, 6 H). ^{13}C NMR ($CDCl_3$, 100 MHz): δ 144.0, 141.1, 140.4, 136.4, 136.0, 130.0, 124.3, 36.6, 31.9, 31.0, 29.8, 29.7, 29.66, 29.6, 29.4, 22.7, 14.1, −7.97. HRMS (FAB, $C_{44}H_{72}Se_2Sn_2$): calcd, 1000.2008; found, 1000.2005.

Synthesis of Copolymer PαNDSDTFBT. To a 50 mL round-bottomed flask were added Sn-4,9-α-aNDS (140 mg, 0.14 mmol), Br-DTFBT (132.5 mg, 0.14 mmol), $Pd_2(dba)_3$ (5.15 mg, 0.0056 mmol), tri(*o*-tolyl)phosphine (13.69 mg, 0.045 mmol) and dry chlorobenzene (5.8 mL). The mixture was degassed, and the reaction was carried out in the focused microwave instrument under 270 W at 180 °C for 50 min. To end-cap the resultant copolymer, tributyl(thiophen-2-yl)stannane (26.22 mg, 0.07 mmol) was added to the mixture, and the microwave reaction was continued for 10 min under 270 W. Subsequent to the addition of tributyl(thiophen-2-yl)stannane, another end-capping reagent, 2-bromothiophene (12.37 mg, 0.076 mmol) was added, and the reaction was continued for another 10 min. The mixture was added into methanol dropwise. The precipitate was collected by filtration and washed by Soxhlet extraction with acetone and hexane sequentially for 3 days. The crude polymer was dissolved in hot chloroform, and the residual Pd catalyst and Sn metal was removed by Pd-thiol gel and Pd-TAAcOH (Silicycle Int.). After filtration and removal of the solution, the polymer was redissolved in THF and reprecipitated by methanol. The resultant polymer was collected by filtration, and dried under vacuum to afford a dark-blue fiber-like solid (200 mg, 98%, M_n = 33 300, PDI = 1.29). Anal. Calcd for $C_{84}H_{122}F_2N_2S_3Se_2$ (a repeating unit of PαNDSDTFBT): C, 69.48; H, 8.47; N, 1.93. Found: C, 67.49; H, 8.22; N, 1.76.

Synthesis of Copolymer PαNDSDPP. To a 50 mL round-bottomed flask were added Sn-4,9-α-aNDS (134 mg, 0.134 mmol), Br-DPP (137.1 mg, 0.134 mmol), $Pd_2(dba)_3$ (4.93 mg, 0.0054 mmol), tri(*o*-tolyl)phosphine (13.1 mg, 0.043 mmol) and dry chlorobenzene (5.6 mL). The mixture was degassed, and the reaction was carried out in the focused microwave instrument under 270 W at 180 °C for 50 min. To end-cap the resultant copolymer, tributyl(thiophen-2-yl)stannane (25.09 mg, 0.067 mmol) was added to the mixture, and the microwave reaction was continued for 10 min under 270 W. Subsequent to the addition of tributyl(thiophen-2-yl)stannane, another end-capping reagent, 2-bromothiophene (11.84 mg, 0.073 mmol) was added, and the reaction was continued for another 10 min. The mixture was added into methanol dropwise. The precipitate was collected by filtration and washed by Soxhlet extraction with acetone and hexane sequentially for 3 days. The crude polymer was dissolved in hot chloroform, and the residual Pd catalyst and Sn metal was removed by Pd-thiol gel and Pd-TAAcOH (Silicycle Int.). After filtration and removal of the solution, the polymer was redissolved in hot chloroform and reprecipitated by methanol. The resultant polymer was collected by filtration, and dried under vacuum to afford a dark-green fiber-like solid (203 mg, 98%, M_n = 373 900, PDI = 1.97). Anal. Calcd for $C_{92}H_{140}N_2O_2S_2Se_2$ (a repeating unit of PαNDSDPP): C, 72.31; H, 9.23; N, 1.83. Found: C, 70.00; H, 9.07; N, 1.66.

Bottom-Gate/Top-Contact OFET Devices. An *n*-type heavily doped Si wafer with a SiO_2 layer of 300 nm and a capacitance of 11 nF/cm^2 was used as the gate electrode and dielectric layer. The substrates were cleaned by ultrasonication in deionized water, acetone and isopropyl alcohol for 15 min each, and then dried using a N_2 stream. After exposed to UV/ozone for 20 min, the substrates were modified with an octadecyltrichlorosilane (ODTS) self-assembled monolayer. Thin films (40−60 nm in thickness) of polymers were deposited on ODTS-treated SiO_2/Si substrates. The thin films were annealed at 200 °C for 10 min. Gold source and drain contact (40 nm in thickness) were deposited by vacuum evaporation on the organic layer through a shadow mask. Electrical measurements of OTFT devices were carried out at room temperature in air using a 4156C, Agilent Technologies. The field-effect mobility was calculated in the saturation regime by using the equation $I_{ds} = (\mu WC_i/2L)(V_g - V_t)^2$, where I_{ds} is the drain-source current, μ is the field-effect mobility, W is the channel width (1 mm), L is the channel length (100 μm), Ci is the capacitance per unit area of the gate dielectric layer, V_g is the gate voltage and V_t is threshold voltage.

DOI: 10.1021/acs.chemmater.6b02042
Chem. Mater. XXXX, XXX, XXX−XXX

■ ASSOCIATED CONTENT

Supporting Information

The Supporting Information is available free of charge on the ACS Publications website at DOI: 10.1021/acs.chemmater.6b02042.

X-ray crystallography (CIF) of 4,9-α-aNDS (CIF).

Computational details, experimental procedures, and ^{1}H and ^{13}C NMR spectra (PDF).

■ AUTHOR INFORMATION

Corresponding Authors

*Y.-J. Cheng. Email: yjcheng@mail.nctu.edu.tw.

*C.-S. Hsu. Email: cshsu@mail.nctu.edu.tw.

Funding

Ministry of Science and Technology, Taiwan. 104-2113-M-009-013 -MY3.

Notes

The authors declare no competing financial interest.

■ ACKNOWLEDGMENTS

We thank the Ministry of Science and Technology and the Ministry of Education, and Center for Interdisciplinary Science (CIS) of the National Chiao Tung University, Taiwan, for financial support. We thank the National Center of High-performance Computing (NCHC) in Taiwan for computer time and facilities. We thank Prof. Sue-Lein Wang at National Tsing Hua University (NTHU) for help with the X-ray crystallography. We also thank the National Synchrotron Radiation Research Center (NSRRC), and Dr. U-Ser Jeng and Dr. Chun-Jen Su in at BL23A1 station for the help with the GIXS experiments. Y.-J.C thanks the support from the Golden-Jade fellowship of the Kenda Foundation, Taiwan.

■ REFERENCES

(1) Goldfinger, M. B.; Swager, T. M. Fused Polycyclic Aromatics via Electrophile-Induced Cyclization Reactions: Application to the Synthesis of Graphite Ribbons. *J. Am. Chem. Soc.* **1994**, *116*, 7895−7896.

(2) Goldfinger, M. B.; Crawford, K. B.; Swager, T. M. Directed Electrophilic Cyclizations: Efficient Methodology for the Synthesis of Fused Polycyclic Aromatics. *J. Am. Chem. Soc.* **1997**, *119*, 4578−4593.

(3) Forster, M.; Annan, K. O.; Scherf, U. Conjugated Ladder Polymers Containing Thienylene Units. *Macromolecules* **1999**, *32*, 3159−3162.

(4) Scherf, U. Ladder-type Materials. *J. Mater. Chem.* **1999**, *9*, 1853−1864.

(5) Freund, T.; Muellen, K.; Scherf, U. Soluble, High Molecular Weight Ladder Polymers Possessing a Poly(phenylene sulfide) Backbone. *Macromolecules* **1995**, *28*, 547−551.

(6) Jacob, J.; Sax, S.; Piok, T.; List, E. J. W.; Grimsdale, A. C.; Müllen, K. Ladder-Type Pentaphenylenes and Their Polymers: Efficient Blue-Light Emitters and Electron-Accepting Materials via a Common Intermediate. *J. Am. Chem. Soc.* **2004**, *126*, 6987−6995.

(7) Zheng, Q.; Jung, B. J.; Sun, J.; Katz, H. E. Ladder-Type Oligo-p-phenylene-Containing Copolymers with High Open-Circuit Voltages and Ambient Photovoltaic Activity. *J. Am. Chem. Soc.* **2010**, *132*, 5394−5404.

(8) Facchetti, A. π-Conjugated Polymers for Organic Electronics and Photovoltaic Cell Applications. *Chem. Mater.* **2011**, *23*, 733−758.

(9) Guo, X.; Ortiz, R. P.; Zheng, Y.; Hu, Y.; Noh, Y.-Y.; Baeg, K.-J.; Facchetti, A.; Marks, T. J. Bithiophene-Imide-Based Polymeric Semiconductors for Field-Effect Transistors: Synthesis, Structure−Property Correlations, Charge Carrier Polarity, and Device Stability. *J. Am. Chem. Soc.* **2011**, *133*, 1405−1418.

(10) Ashraf, R. S.; Chen, Z.; Leem, D. S.; Bronstein, H.; Zhang, W.; Schroeder, B.; Geerts, Y.; Smith, J.; Watkins, S.; Anthopoulos, T. D.; Sirringhaus, H.; de Mello, J. C.; Heeney, M.; McCulloch, I. Silaindacenodithiophene Semiconducting Polymers for Efficient Solar Cells and High-Mobility Ambipolar Transistors. *Chem. Mater.* **2011**, *23*, 768−770.

(11) Zhang, M.; Guo, X.; Wang, X.; Wang, H.; Li, Y. Synthesis and Photovoltaic Properties of D−A Copolymers Based on Alkyl-Substituted Indacenodithiophene Donor Unit. *Chem. Mater.* **2011**, *23*, 4264−4270.

(12) Cheng, Y.-J.; Cheng, S.-W.; Chang, C.-Y.; Kao, W.-S.; Liao, M.-H.; Hsu, C.-S. Diindenothieno[2,3-b]thiophene Aarene for Efficient Organic Photovoltaics with an Extra High Open-Circuit Voltage of 1.14 eV. *Chem. Commun.* **2012**, *48*, 3203−3205.

(13) Cheng, Y.-J.; Ho, Y.-J.; Chen, C.-H.; Kao, W.-S.; Wu, C.-E.; Hsu, S.-L.; Hsu, C.-S. Synthesis, Photophysical and Photovoltaic Properties of Conjugated Polymers Containing Fused Donor−Acceptor Dithienopyrrolobenzothiadiazole and Dithienopyrroloquinoxaline Arenes. *Macromolecules* **2012**, *45*, 2690−2698.

(14) Chen, C.-H.; Cheng, Y.-J.; Chang, C.-Y.; Hsu, C.-S. Donor−Acceptor Random Copolymers Based on a Ladder-Type Nonacyclic Unit: Synthesis, Characterization, and Photovoltaic Applications. *Macromolecules* **2011**, *44*, 8415−8424.

(15) Chang, H.-H.; Tsai, C.-E.; Lai, Y.-Y.; Chiou, D.-Y.; Hsu, S.-L.; Hsu, C.-S.; Cheng, Y.-J. Synthesis, Molecular and Photovoltaic Properties of Donor−Acceptor Conjugated Polymers Incorporating a New Heptacylic Indacenodithieno[3,2-*b*]thiophene Arene. *Macromolecules* **2012**, *45*, 9282−9291.

(16) Lei, T.; Wang, J.-Y.; Pei, J. Design, Synthesis, and Structure−Property Relationships of Isoindigo-Based Conjugated Polymers. *Acc. Chem. Res.* **2014**, *47*, 1117−1126.

(17) Wu, J.-S.; Cheng, S.-W.; Cheng, Y.-J.; Hsu, C.-S. Donor-Acceptor Conjugated Polymers Based on Multifused Ladder-Type Arenes for Organic Solar Cells. *Chem. Soc. Rev.* **2015**, *44*, 1113−1154.

(18) Matthews, J. R.; Niu, W.; Tandia, A.; Wallace, A. L.; Hu, J.; Lee, W.-Y.; Giri, G.; Mannsfeld, S. C. B.; Xie, Y.; Cai, S.; Fong, H. H.; Bao, Z.; He, M. Scalable Synthesis of Fused Thiophene-Diketopyrrolopyrrole Semiconducting Polymers Processed from Nonchlorinated Solvents into High Performance Thin Film Transistors. *Chem. Mater.* **2013**, *25*, 782−789.

(19) Mei, J.; Kim, D. H.; Ayzner, A. L.; Toney, M. F.; Bao, Z. Siloxane-Terminated Solubilizing Side Chains: Bringing Conjugated Polymer Backbones Closer and Boosting Hole Mobilities in Thin-Film Transistors. *J. Am. Chem. Soc.* **2011**, *133*, 20130−20133.

(20) Hou, J.; Park, M.-H.; Zhang, S.; Yao, Y.; Chen, L.-M.; Li, J.-H.; Yang, Y. Bandgap and Molecular Energy Level Control of Conjugated Polymer Photovoltaic Materials Based on Benzo[1,2-*b*:4,5-*b*′]-dithiophene. *Macromolecules* **2008**, *41*, 6012−6018.

(21) Liang, Y.; Xu, Z.; Xia, J.; Tsai, S.-T.; Wu, Y.; Li, G.; Ray, C.; Yu, L. For the Bright Future—Bulk Heterojunction Polymer Solar Cells with Power Conversion Efficiency of 7.4%. *Adv. Mater.* **2010**, *22*, E135−E138.

(22) Liang, Y.; Yu, L. A New Class of Semiconducting Polymers for Bulk Heterojunction Solar Cells with Exceptionally High Performance. *Acc. Chem. Res.* **2010**, *43*, 1227−1236.

(23) Zhou, H.; Yang, L.; Stuart, A. C.; Price, S. C.; Liu, S.; You, W. Development of Fluorinated Benzothiadiazole as a Structural Unit for a Polymer Solar Cell of 7% Efficiency. *Angew. Chem., Int. Ed.* **2011**, *50*, 2995−2998.

(24) Ye, L.; Zhang, S.; Huo, L.; Zhang, M.; Hou, J. Molecular Design Toward Highly Efficient Photovoltaic Polymers Based on Two-Dimensional Conjugated Benzodithiophene. *Acc. Chem. Res.* **2014**, *47*, 1595−1603.

(25) Subbiah, J.; Purushothaman, B.; Chen, M.; Qin, T.; Gao, M.; Vak, D.; Scholes, F. H.; Chen, X.; Watkins, S. E.; Wilson, G. J.; Holmes, A. B.; Wong, W. W. H.; Jones, D. J. Organic Solar Cells Using a High-Molecular-Weight Benzodithiophene−Benzothiadiazole Copolymer with an Efficiency of 9.4%. *Adv. Mater.* **2015**, *27*, 702−705.

DOI: 10.1021/acs.chemmater.6b02042
Chem. Mater. XXXX, XXX, XXX−XXX

(26) Chen, M.-C.; Kim, C.; Chen, S.-Y.; Chiang, Y.-J.; Chung, M.-C.; Facchetti, A.; Marks, T. J. Functionalized Anthradithiophenes for Organic Field-Effect Transistors. *J. Mater. Chem.* **2008**, *18*, 1029−1036.
(27) Lehnherr, D.; Waterloo, A. R.; Goetz, K. P.; Payne, M. M.; Hampel, F.; Anthony, J. E.; Jurchescu, O. D.; Tykwinski, R. R. Isomerically Pure *syn*-Anthradithiophenes: Synthesis, Properties, and FET Performance. *Org. Lett.* **2012**, *14*, 3660−3663.
(28) Mamada, M.; Minamiki, T.; Katagiri, H.; Tokito, S. Synthesis, Physical Properties, and Field-Effect Mobility of Isomerically Pure *syn*-/*anti*-Anthradithiophene Derivatives. *Org. Lett.* **2012**, *14*, 4062−4065.
(29) Wu, J.-S.; Lin, C.-T.; Wang, C.-L.; Cheng, Y.-J.; Hsu, C.-S. New Angular-Shaped and Isomerically Pure Anthradithiophene with Lateral Aliphatic Side Chains for Conjugated Polymers: Synthesis, Characterization, and Implications for Solution-Prossessed Organic Field-Effect Transistors and Photovoltaics. *Chem. Mater.* **2012**, *24*, 2391−2399.
(30) Subramanian, S.; Park, S. K.; Parkin, S. R.; Podzorov, V.; Jackson, T. N.; Anthony, J. E. Chromophore Fluorination Enhances Crystallization and Stability of Soluble Anthradithiophene Semiconductors. *J. Am. Chem. Soc.* **2008**, *130*, 2706−2707.
(31) Payne, M. M.; Parkin, S. R.; Anthony, J. E.; Kuo, C.-C.; Jackson, T. N. Organic Field-Effect Transistors from Solution-Deposited Functionalized Acenes with Mobilities as High as 1 $cm^2/V{\cdot}s$. *J. Am. Chem. Soc.* **2005**, *127*, 4986−4987.
(32) Jiang, Y.; Mei, J.; Ayzner, A. L.; Toney, M. F.; Bao, Z. 5,11-Conjugation-Extended Low-Bandgap Anthradithiophene-Containing Polymer Exhibiting Enhanced Thin-Film Order and Field-Effect Mobility. *Chem. Commun.* **2012**, *48*, 7286−7288.
(33) Shinamura, S.; Osaka, I.; Miyazaki, E.; Nakao, A.; Yamagishi, M.; Takeya, J.; Takimiya, K. Linear- and Angular-Shaped Naphthodithiophenes: Selective Synthesis, Properties, and Application to Organic Field-Effect Transistors. *J. Am. Chem. Soc.* **2011**, *133*, 5024−5035.
(34) Osaka, I.; Abe, T.; Shimawaki, M.; Koganezawa, T.; Takimiya, K. Naphthodithiophene-Based Donor−Acceptor Polymers: Versatile Semiconductors for OFETs and OPVs. *ACS Macro Lett.* **2012**, *1*, 437−440.
(35) Shinamura, S.; Sugimoto, R.; Yanai, N.; Takemura, N.; Kashiki, T.; Osaka, I.; Miyazaki, E.; Takimiya, K. Orthogonally Functionalized Naphthodithiophenes: Selective Protection and Borylation. *Org. Lett.* **2012**, *14*, 4718−4721.
(36) Osaka, I.; Shinamura, S.; Abe, T.; Takimiya, K. Naphthodithiophenes as Building Units for Small Molecules to Polymers; a Case Study for in-Depth Understanding of Structure−Property Relationships in Organic Semiconductors. *J. Mater. Chem. C* **2013**, *1*, 1297−1304.
(37) Cheng, S.-W.; Tsai, C.-E.; Liang, W.-W.; Chen, Y.-L.; Cao, F.-Y.; Hsu, C.-S.; Cheng, Y.-J. Angular-Shaped 4,9-Dialkylnaphthodithiophene-Based Donor−Acceptor Copolymers for Efficient Polymer Solar Cells and High-Mobility Field-Effect Transistors. *Macromolecules* **2015**, *48*, 2030−2038.
(38) Osaka, I.; Kakara, T.; Takemura, N.; Koganezawa, T.; Takimiya, K. Naphthodithiophene-Naphthobisthiadiazole Copolymers for Solar Cells: Alkylation Drives the Polymer Backbone Flat and Promotes Efficiency. *J. Am. Chem. Soc.* **2013**, *135*, 8834−8837.
(39) Osaka, I.; Houchin, Y.; Yamashita, M.; Kakara, T.; Takemura, N.; Koganezawa, T.; Takimiya, K. Contrasting Effect of Alkylation on the Ordering Structure in Isomeric Naphthodithiophene-Based Polymers. *Macromolecules* **2014**, *47*, 3502−3510.
(40) Cheng, S.-W.; Chiou, D.-Y.; Lai, Y.-Y.; Yu, R.-H.; Lee, C.-H.; Cheng, Y.-J. Synthesis and Molecular Properties of Four Isomeric Dialkylated Angular-Shaped Naphthodithiophenes. *Org. Lett.* **2013**, *15*, 5338−5341.
(41) Osaka, I.; Abe, T.; Shinamura, S.; Takimiya, K. Impact of Isomeric Structures on Transistor Performances in Naphthodithiophene Semiconducting Polymers. *J. Am. Chem. Soc.* **2011**, *133*, 6852−6860.
(42) Cheng, S.-W.; Chiou, D.-Y.; Tsai, C.-E.; Liang, W.-W.; Lai, Y.-Y.; Hsu, J.-Y.; Hsu, C.-S.; Osaka, I.; Takimiya, K.; Cheng, Y.-J. Angular-Shaped 4,9-Dialkyl α- and β-Naphthodithiophene-Based Donor-Acceptor Copolymers: Investigation of Isomeric Structural Effects on Molecular Properties and Performance of Field-Effect Transistors and Photovoltaics. *Adv. Funct. Mater.* **2015**, *25*, 6131−6143.
(43) Takimiya, K.; Kunugi, Y.; Konda, Y.; Niihara, N.; Otsubo, T. 2,6-Diphenylbenzo[1,2-*b*:4,5-*b*′]dichalcogenophenes: A New Class of High-Performance Semiconductors for Organic Field-Effect Transistors. *J. Am. Chem. Soc.* **2004**, *126*, 5084−5085.
(44) Takimiya, K.; Konda, Y.; Ebata, H.; Otsubo, T.; Kunugi, Y. Organic Field-Effect Transistors Based on 2,6-Diphenylbenzo [1,2-*b*:5,4-*b*′]-Dithiophene and -Diselenophene (iso-DPh-BDXs). *Mol. Cryst. Mol. Cryst. Liq. Cryst.* **2006**, *455*, 361−365.
(45) Ballantyne, A. M.; Chen, L.; Nelson, J.; Bradley, D. D. C.; Astuti, Y.; Maurano, A.; Shuttle, C. G.; Durrant, J. R.; Heeney, M.; Duffy, W.; McCulloch, I. Studies of Highly Regioregular Poly(3-hexylselenophene) for Photovoltaic Applications. *Adv. Mater.* **2007**, *19*, 4544−4547.
(46) Chen, Z.; Lemke, H.; Albert-Seifried, S.; Caironi, M.; Nielsen, M. M.; Heeney, M.; Zhang, W.; McCulloch, I.; Sirringhaus, H. High Mobility Ambipolar Charge Transport in Polyselenophene Conjugated Polymers. *Adv. Mater.* **2010**, *22*, 2371−2375.
(47) Li, L.; Hollinger, J.; Jahnke, A. A.; Petrov, S.; Seferos, D. S. Polyselenophenes with Distinct Crystallization Properties. *Chem. Sci.* **2011**, *2*, 2306−2310.
(48) Patra, A.; Wijsboom, Y. H.; Leitus, G.; Bendikov, M. Tuning the Band Gap of Low-Band-Gap Polyselenophenes and Polythiophenes: The Effect of the Heteroatom. *Chem. Mater.* **2011**, *23*, 896−906.
(49) Nakano, M.; Mori, H.; Shinamura, S.; Takimiya, K. Naphtho-[2,3-*b*:6,7-*b*′]dichalcogenophenes: Syntheses, Characterizations, and Chalcogene Atom Effects on Organic Field-Effect Transistor and Organic Photovoltaic Devices. *Chem. Mater.* **2012**, *24*, 190−198.
(50) Chang, H.-H.; Tsai, C.-E.; Lai, Y.-Y.; Liang, W.-W.; Hsu, S.-L.; Hsu, C.-S.; Cheng, Y.-J. A New Pentacyclic Indacenodiselenophene Arene and Its Donor−Acceptor Copolymers for Solution-Processable Polymer Solar Cells and Transistors: Synthesis, Characterization, and Investigation of Alkyl/Alkoxy Side-Chain Effect. *Macromolecules* **2013**, *46*, 7715−7726.
(51) Hollinger, J.; Gao, D.; Seferos, D. S. Selenophene Electronics. *Isr. J. Chem.* **2014**, *54*, 440−453.
(52) Jeffries-El, M.; Kobilka, B. M.; Hale, B. J. Optimizing the Performance of Conjugated Polymers in Organic Photovoltaic Cells by Traversing Group 16. *Macromolecules* **2014**, *47*, 7253−7271.
(53) Kim, K.-H.; Park, S.; Yu, H.; Kang, H.; Song, I.; Oh, J. H.; Kim, B. J. Determining Optimal Crystallinity of Diketopyrrolopyrrole-Based Terpolymers for Highly Efficient Polymer Solar Cells and Transistors. *Chem. Mater.* **2014**, *26*, 6963−6970.
(54) Ashraf, R. S.; Meager, I.; Nikolka, M.; Kirkus, M.; Planells, M.; Schroeder, B. C.; Holliday, S.; Hurhangee, M.; Nielsen, C. B.; Sirringhaus, H.; McCulloch, I. Chalcogenophene Comonomer Comparison in Small Band Gap Diketopyrrolopyrrole-Based Conjugated Polymers for High-Performing Field-Effect Transistors and Organic Solar Cells. *J. Am. Chem. Soc.* **2015**, *137*, 1314−1321.
(55) Lai, Y.-Y.; Chang, H.-H.; Lai, Y.-Y.; Liang, W.-W.; Tsai, C.-E.; Cheng, Y.-J. Angular-Shaped 4,10-Dialkylanthradiselenophene and Its Donor−Acceptor Conjugated Polymers: Synthesis, Physical, Transistor, and Photovoltaic Properties. *Macromolecules* **2015**, *48*, 6994−7006.
(56) Heeney, M.; Zhang, W.; Crouch, D. J.; Chabinyc, M. L.; Gordeyev, S.; Hamilton, R.; Higgins, S. J.; McCulloch, I.; Skabara, P. J.; Sparrowe, D.; Tierney, S. Regioregular Poly(3-hexyl)selenophene: a Low Band Gap Organic Hole Transporting Polymer. *Chem. Commun.* **2007**, *43*, 5061−5063.
(57) Zade, S. S.; Zamoshchik, N.; Bendikov, M. Oligo- and Polyselenophenes: A Theoretical Study. *Chem. - Eur. J.* **2009**, *15*, 8613−8624.
(58) Patra, A.; Bendikov, M. Polyselenophenes. *J. Mater. Chem.* **2010**, *20*, 422−433.

DOI: 10.1021/acs.chemmater.6b02042
Chem. Mater. XXXX, XXX, XXX−XXX

(59) Bedi, A.; Debnath, S.; Zade, S. S. Diselenolodiselenole: a Selenium Containing Fused Heterocycle for Conjugated Systems. *Chem. Commun.* **2014**, *50*, 13454−13456.
(60) Chen, J.-M.; Santra, B. K.; Liu, C. W. Intermolecular Se···Se interactions Observed in Indium Compounds Containing Dialkyl Diselenophosphate Ligands: Syntheses, Structure, and Solution Studies of [In{Se2P(OR)2}3] (R = Et, iPr). *Inorg. Chem. Commun.* **2004**, *7*, 1103−1105.
(61) Hartman, I.; Raia, C. A.; Zauhar, R. J. Evidence for a Strong Selenium−Aromatic Interaction Derived from Crystallographic Data and ab Initio Quantum Chemical Calculations. *Biopolymers* **2006**, *83*, 595−613.
(62) Shinamura, S.; Miyazaki, E.; Takimiya, K. Synthesis, Properties, Crystal Structures, and Semiconductor Characteristics of Naphtho[1,2-*b*:5,6-*b*′]dithiophene and -diselenophene Derivatives. *J. Org. Chem.* **2010**, *75*, 1228−1234.
(63) Nakano, M.; Shinamura, S.; Sugimoto, R.; Osaka, I.; Miyazaki, E.; Takimiya, K. Borylation on Benzo[1,2-*b*:4,5-*b*′]- and Naphtho[1,2-*b*:5,6-*b*′]dichalcogenophenes: Different Chalcogene Atom Effects on Borylation Reaction Depending on Fused Ring Structure. *Org. Lett.* **2012**, *14*, 5448−5451.
(64) Xu, J.; Wang, Y.; Burton, D. J. Site-Specific Preparation of 3-Fluoro-1-Substituted-Naphthalenes via a Novel Base-Catalyzed Cyclization Reaction from (E)-Monofluoroenynes§. *Org. Lett.* **2006**, *8*, 2555−2558.
(65) Mitoraj, M. P.; Michalak, A.; Ziegler, T. A Combined Charge and Energy Decomposition Scheme for Bond Analysis. *J. Chem. Theory Comput.* **2009**, *5*, 962−975.
(66) Mitoraj, M. P.; Michalak, A.; Ziegler, T. On the Nature of the Agostic Bond between Metal Centers and β-Hydrogen Atoms in Alkyl Complexes. An Analysis Based on the Extended Transition State Method and the Natural Orbitals for Chemical Valence Scheme (ETS-NOCV). *Organometallics* **2009**, *28*, 3727−3733.
(67) Kurczab, R.; Mitoraj, M. P.; Michalak, A.; Ziegler, T. Theoretical Analysis of the Resonance Assisted Hydrogen Bond Based on the Combined Extended Transition State Method and Natural Orbitals for Chemical Valence Scheme. *J. Phys. Chem. A* **2010**, *114*, 8581−8590.
(68) Ringer, A. L.; Sinnokrot, M. O.; Lively, R. P.; Sherrill, C. D. The Effect of Multiple Substituents on Sandwich and T-Shaped π−π Interactions. *Chem. - Eur. J.* **2006**, *12*, 3821−3828.
(69) Sinnokrot, M. O.; Sherrill, C. D. High-Accuracy Quantum Mechanical Studies of π−π Interactions in Benzene Dimers. *J. Phys. Chem. A* **2006**, *110*, 10656−10668.
(70) Sherrill, C. D. Energy Component Analysis of π Interactions. *Acc. Chem. Res.* **2013**, *46*, 1020−1028.
(71) Getmanenko, Y. A.; Tongwa, P.; Timofeeva, T. V.; Marder, S. R. Base-Catalyzed Halogen Dance Reaction and Oxidative Coupling Sequence as a Convenient Method for the Preparation of Dihalobisheteroarenes. *Org. Lett.* **2010**, *12*, 2136−2139.

DOI: 10.1021/acs.chemmater.6b02042
Chem. Mater. XXXX, XXX, XXX−XXX